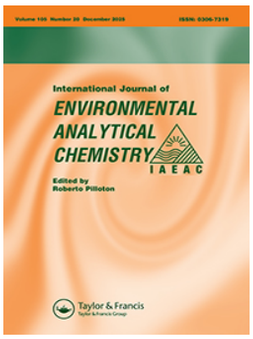

International Journal of Environmental Analytical Chemistry

ISSN: 0306-7319 (Print) 1029-0397 (Online) Journal homepage: www.tandfonline.com/journals/geac20

# Pumice modified with didodecyldimethylammonium bromide as a cost-effective, eco-friendly adsorbent for Cr(VI)

Ismail M. Ahmed, AbdElaziz A. Nayl, Weal A.A. Arafa, Hassan M.A. Hassan, Ahmed I. Abd-Elhamid, Ashraf A. Aly & Stefan Bräse

**To cite this article:** Ismail M. Ahmed, AbdElaziz A. Nayl, Weal A.A. Arafa, Hassan M.A. Hassan, Ahmed I. Abd-Elhamid, Ashraf A. Aly & Stefan Bräse (2025) Pumice modified with didodecyldimethylammonium bromide as a cost-effective, eco-friendly adsorbent for Cr(VI), International Journal of Environmental Analytical Chemistry, 105:20, 8600-8624, DOI: 10.1080/03067319.2025.2479582

**To link to this article:** https://doi.org/10.1080/03067319.2025.2479582

INTERNATIONAL JOURNAL OF ENVIRONMENTAL ANALYTICAL CHEMISTRY
2025, VOL. 105, NO. 20, 8600–8624
https://doi.org/10.1080/03067319.2025.2479582

Taylor & Francis
Taylor & Francis Group



# Pumice modified with didodecyldimethylammonium bromide as a cost-effective, eco-friendly adsorbent for Cr(VI)

Ismail M. Ahmed[a], AbdElaziz A. Nayl[a], Weal A.A. Arafa[a], Hassan M.A. Hassan[a], Ahmed I. Abd-Elhamid[b], Ashraf A. Aly[c] and Stefan Bräse[d]

[a]Department of Chemistry, College of Science, Jouf University, Sakaka, Saudi Arabia; [b]Composites and Nanostructured Materials Research Department, Advanced Technology and New Materials Research Institute, City of Scientific Research and Technological Applications (SRTA-City), NewBorgAl-Arab, Egypt; [c]Chemistry Department, Faculty of Science, Organic Division, Minia University, Minya, Egypt; [d]Institute of Biological and Chemical Systems – Functional Molecular Systems (IBCS-FMS), Karlsruhe, Germany

**ABSTRACT**

Various types of organically modified minerals have already attracted the attention of researchers due to their promising and environmentally friendly properties and their diverse application. This study aims to develop a cost-effective and efficient adsorbent for Cr(VI) removal from wastewater by modifying pumice with acid activation and cationic surfactant treatment. The research focuses on optimising adsorption conditions, understanding the adsorption mechanisms, and evaluating the material's reusability for large-scale applications. This study improves the properties of pumice (Pmc), surface organomodification using 5 M $H_2SO_4$ activation and a double-chain cationic surface active agent as an organic modifier, didodecyldimethylammonium bromide (DDAB) for the sorption of Cr(VI). Physicochemical characteristics of natural-pumice and organo-modified one were studied by EDX, SEM, FTIR, TGA, DTA, XRD and $N_2$ adsorption/desorption tools. The influence of time, Cr(VI) concentrations, solution pH, weight of adsorbent, and temperature were measured and discussed in batch equilibration technique. The results showed rapid adsorption (60 min) with optimal efficiency at pH = 2 for Cr(VI) anions. The removal data fitted the Langmuir model, with a maximum adsorption capacity of 7.81 mg/g. The sorption of these anions onto DDAB/Pmc followed pseudo-second-order rates. Thermodynamic parameters for anions adsorption have been evaluated. The parameters gained from experiments and others can be utilised to design an economical treatment plant for water polluted with Cr(VI) anions or wastewater resulting from industrial.

**ARTICLE HISTORY**
Received 25 January 2025
Accepted 10 March 2025

**KEYWORDS**
Cr(VI); adsorption; double-chain surface active agent; pumice composite

## 1. Introduction

Heavy metal species pose severe risks to human health and the environment [1], with chromium being a major contaminant in various industries [1,2]. Cr(VI) is highly toxic,

**CONTACT** Ismail M. Ahmed imibrahim@ju.edu.sa; Stefan Bräse stefan.braese@kit.edu
Supplemental data for this article can be accessed online at https://doi.org/10.1080/03067319.2025.2479582

causing skin rashes, ulcers, genetic mutations, liver damage and cancer [1–3]. According to the US EPA, the safe limit for total chromium in drinking water is 0.1 ppm, while Cr(VI) should not exceed 0.05 ppm. However, industrial wastewater, especially from tanneries and electroplating, can contain Cr(VI) levels as high as 1500 ppm, making its removal essential [4,5]. Several approaches have been explored for the in-situ treatment of industrial and domestic wastewater to remove Cr(VI) species, including flocculation and precipitation, membranes, redox, microbes, electro-chemistry, ion-exchange and adsorption methods [2–10]. Ion exchange and adsorption are appropriate technologies for any impurities subtraction from wastewater; as a result, it has the benefits of a low budget, simple employment and great effectiveness [9,10]. The removal of chromium ions from water is essential, with sorption being an effective and superior treatment method. It is practical, efficient, and does not produce toxic byproducts [10–14]. Various types of solid-phase adsorbents, including modified and unmodified activated carbons and their derivatives, as well as zeolite, MOFs, clay, and mineral particles, have been investigated and utilised [6,7]. Compared with further adsorbents, clay and minerals with physical-adsorption capacity and surface chemical reactivity are readily obtainable, making them a growing focus as of late [7–9]. A wide range of commercial solid materials, such as activated carbon, resins and chelating polymers, is available for ion adsorption; however, they are relatively expensive [1–7]. Abundant little-rate natural solids have been recommended as would-be sources of cost-effective artificial sorbents [7,8]. Natural low-cost solids that have been intended include green algae, leaf mould, moss peat, wood, coconut rescue waste, activated charcoals, char fibres, rubber, etc. [6]. Still, different cheap, effortlessly obtainable and extremely effective adsorbent solids are required.

In recent studies, research on low-cost clays, natural ores, and rock-based sorbents has expanded, leading to the utilisation of various ores and solid minerals for the removal of metal ions, i.e. iron oxide, silica, quartz, kaolinite, zeolite, clay minerals and pumice particles [7–16]. Although these solid materials have lower adsorption capabilities than synthesised ion exchangers, their significantly lower cost makes them promising for removing heavy metal ions from water and wastewater [8–11]. These adsorbents (clay and natural minerals) can work as they are or in modified new forms [17]. Organomodification, the attachment of organic species to clay or mineral surfaces, creates highly efficient composites. These composites offer enhanced properties and diverse applications [17].

Pumice stone is a porous volcanic rock with a large surface area, composed of finely vesicular pyroclastic glass. It forms when volcanic gases nucleate into bubbles within viscous magma before cooling into glass. With an average porosity of 90%, pumice often floats on water initially. In addition to its practical applications in wastewater treatment, pumice has been widely studied for its effectiveness as a sorbent, filtration medium, bed material, and support media [15,16]. Research showed that unmodified pumice cannot remove phenolic species, whereas organo-modified pumice is an excellent sorbent. Experimental results confirm its high efficiency in phenolic species adsorption [18]. Meanwhile, pumice is a little charge solid material besides an absorbent assembly and huge surface area that is commonly obtainable and can be certainly treated and adapted; adapted pumice stone particles would be an appropriate applicant as an absorbent.

Given the advantages of organo-modified pumice, its potential for removing other pollutants, such as chromate species, should be explored. To our knowledge, the use

of double-chain surfactant-modified pumice for chromate removal has not been studied, we investigate the surface organomodification of pumice through acid activation using 5 M $H_2SO_4$ followed by functionalisation with DDAB. The physicochemical properties of both natural (Pmc) and modified pumice (DDAB/Pmc) were characterised to evaluate the impact of modification on the mineral's surface properties. Batch adsorption experiments examined key parameters affecting $Cr^{6+}$ removal, including contact time, pH, and temperature. Kinetic and equilibrium data were analysed using pseudo-second-order and Langmuir models, while thermodynamic parameters assessed feasibility and spontaneity. The novelty of this research lies in the dual modification strategy combining $H_2SO_4$ activation with a double-chain cationic surfactant to enhance $Cr^{+6}$ removal efficiency.

## 2. Materials and methods

### 2.1. Chemicals and reagents

Pumice was obtained from the local market. All chemicals were used without any additional purification. To create a 1000 mg/L $Cr^{+6}$ stock solution purchased from Aldrich, about 0.283 g of $K_2Cr_2O_7$ ($K_2Cr_2O_7$, ≥99% purity) was placed in water in a 100-mL flask. Didodecyldimethylammonium bromide (DDAB), a double-chain cationic Surface active agent, was purchased from Sigma-Aldrich with ≥ 98% purity. Sulfuric acid ($H_2SO_4$, ≥98% purity) was employed in the activation process of pumice. The pH of the working solutions was adjusted using sodium hydroxide (NaOH, ≥98% purity) and hydrochloric acid (HCl, ≥37% purity) as required.

### 2.2. Synthesis of DDAB/Pmc composite (organ modification of pumice)

Before use, pumice stone particles were powdered and separated using a 100 mesh-extent sieve to get homogeneous powder; pumice powder was agitated in 5 M $H_2SO_4$ for one day through a ratio of 1:5 filtered, then pumice-activated was washed to pH 7 and dried at about 105°C to a constant mass. After that, 5.0 g of the activated pumice was shaken overnight with 100 mL of 1% DDAB for 24 h. The modified pumice was washed thrice using distilled water overnight and dried at 105°C.

### 2.3. Physical and chemical characteristics of DDAB/Pmc composite

The interaction between DDAB/Pmc and the aqueous phase plays a key role in chromate adsorption. Adsorption efficiency depends on the material's functional groups, chemical structure, and surface properties, which influence the adsorption capacity in aqueous solutions [19]. The crystalline structure of the investigated DDAB/Pmc composite was examined using XRD-7000 at a diffraction angle range of 10–80 and a scan speed of 0.2/min. Shimadzuo DTG-60/60 h thermal analyser has been utilised to measure DTA and TGA where DDAB/Pmc was heated up to 600°C under $N_2$ atmospheric. Functional groups were estimated by IRTracer-100 from Shimadzu, Kyoto, Japan, with a resolution of 4.0 $cm^{-1}$; the sample was estimated between 4000 and 400 cm-1; the sample was estimated between 4000 and 400 cm-1. Morphology of the solids was scanned via Thermo Scientific Quattro

ESEM, and $N_2$Brunauer-Emmett-Teller (BET) surface area analyses were characterised utilising Quantachrome, NOVA 4200 e series).

### 2.4. Batch adsorption experiments

Batch equilibration was utilised to evaluate the adsorption of Cr(VI)via DDAB/Pmc composite, where 0.05 g of the metal mentioned above ions was shaken with 10 mL of Cr(VI) in pHs (2.0–10.0), Cr(VI) concentration was investigated (10–100 $mg.L^{-1}$) where contact-time remained between 5 and 180 min. And the temperature was in the range of 25–55°C. After the mixture had been shaken, the solutions were separated by centrifugation, and the concentration of Cr + 6 was measured spectrophotometrically using a 1,5-diphenylcarbazide scheme (540 nm) [20].

### 2.5. Analysis of data

The % elimination or adsorption (%*R*) of Cr(VI) at steadiness and quantity of Cr(VI) relocated onto DDAB/Pmc surface at time *t* $q_t$ ($mg.g^{-1}$) and at steadiness $q_e$ ($mg.g^{-1}$) were considered via subsequent relationships [19]:

$$R\% = \frac{C_o - Ct}{C_o} \times 100 \tag{1}$$

$$q_t = (C_o - C_t)\frac{V}{m} \tag{2}$$

$$q_e = (C_o - C_e)\frac{V}{m} \tag{3}$$

Somewhere, qt expressions the extent to which Cr(VI) was sorbed onto DDAB/Pmc composite at *t* time. $C_t$ and Ce signify Cr(VI) masses in the solution (mg.l-1) at time t, time 0, and steadiness; correspondingly, Co *and Ce signify Cr(VI) masses in the solution (mg.l-1) at time t, time 0 and steadiness*. Volume *V* (l) and *m* are the weights of the DDAB/Pmc composite (g).

### 2.6. Theoretical background

#### 2.6.1. Modeling of Cr(VI) adsorption

**2.6.1.1. Kinetic modeling.** The kinetics of the treatment scheme offer beneficial insights into the exterior interaction employed in the adsorptive removal of the $Cr^{\pm 6}$ onto DDAB/Pmc [21,22]. Kinetics creates a relationship between contact time and Cr(VI) concentration and incidence implicated in the sorption route. To inspect the mechanism of Cr(VI) sorption via DDAB/Pmc composite, kinetic formulas have been second hand to find likely mechanisms of the sorptive-removal route. In our study here, pseudo-first-order (PFO) [23], -second-order (PSO) [24] and intra-particle diffusion (IPD) [25,26] kinetics equations were recommended as comes after to expose the mechanism of Cr(VI) sorption liable on the DDAB/Pmc characteristics [27]. PFO rate Lagergren model is:

$$\log(q_e - q_t) = \log q_e - \left(\frac{k_1}{2.303}\right)t \tag{4}$$

Wherever $k_1$ is PFO rate-constant ($min^{-1}$) at shaking time $t$ (min.), a linear plot (straight-line) resulting from $log(q_e- q_t)$ *vs.* $t$ proposes the applicability of the PFO model. $q_e$ and $k_1$ could be computed via intercept *vs*. straight line slope. The PSO kinetic equation is stated as:

$$\frac{t}{q_t} = \frac{1}{k_2 q_e^2} + \frac{1}{q_e}t \tag{5}$$

Where $k_2$ is the PSO rate constant ($g.mg^{-1}.min^{-1}$), the plot of $t/q_t$ vs. t ought to generate a linear plot in instance the PSO kinetic equation stays valid, and $q_e$ and $k_2$ can be calculated after obtaining both line plot -intercept and -slope, respectively.

The next calculation can estimate effect of IPD resistance on Cr(VI) species adsorption [28]:

$$q_t = k_3 t^{1/2} + C \tag{6}$$

Wherever $k_3$ is the IPD rate constant ($mg/g.min^{-0.5}$), the $C$ rate provides evidence concerning the value of the boundary layer. According to IPD, the plot of $q_t$ *vs* $t_{0.5}$. has to be linear in case IPD is intricate in Cr(VI) species removal. If this line passes out of origin at that point, IPD is the rate-controlling step [29,30].

***2.6.1.2. Isotherm models.*** Isotherms are numerical forms that count on collections of assumptions that are classically interrelated to sorbents' homogeneity or heterogeneity, concealment, and feasibility of contact over sorbate ion species once the adsorption process ranges a steadiness formal [31]. Langmuir and Freundlich's forms are routinely advantageous for depicting subtraction steadiness for waste-water management [32,33]. Equilibrium statistics grown in our work were similarly valued via the forms above, as has too been applied by diverse studies [34,]. Cr(VI) concentration influence on the uptake of Cr(VI) was calculated under optimised conditions at different [Cr(VI)], from 10–100 $\mu g.mL^{-1}$, and sorption isotherm forms were utilised. Langmuir form could be defined by linearised formula as shadows [35]:

$$\frac{C_e}{q_e} = \frac{1}{bQ_{\max}} + \frac{1}{Q_{\max}} \times C_e \tag{7}$$

$Q_{max}$ and $b$ are the maximum mono-layer capacity (theoretical) and the constant of Langmuir interrelated to sorption energy [36]. The central amount of this model could be stated in expressions of separation factor, $R_{L,}$ that are computed via [37]:

$$R_L = \frac{1}{1 + bC_o} \tag{8}$$

The empirical form of Freundlich form relies on removal happening onto heterogeneous exteriors as follows [38]:

$$\log q_e = \log k_f + \frac{1}{n}\log C_e \tag{9}$$

$K_f$ and $n$ are steadiness values indicating the amount adsorbed and adsorption strength, respectively. All variables of the Freundlich and Langmuir forms can be obtained as in previous published works [32].

#### 2.6.2. Thermodynamic factors

Thermodynamic factors were assessed by determining the necessity of $K_C$ (equilibrium constant) on temperature. ΔG°, ΔH° and ΔS° for Cr(VI) adsorption onto the DDAB/Pmc composite can be intended by Gibbs' free energy and Van't Hoff equations [32,33].

$$\Delta G^{o} = -RT \ln K_C \tag{10}$$

$$K_C = \frac{q_e}{C_e} \tag{11}$$

$$\ln K_C = \frac{\Delta S^{o}}{R} + \frac{-\Delta H^{o}}{R}\frac{1}{T} \tag{12}$$

Wherever $R$ and $T$ are gas constant and temperature. *ΔH could be valued from the can't* Hoff calculation plot, *ln$K_c$ vs. 1/T* [28]. All tests were frequent at the slightest 2 distinct runs, and mean values were stated. Equally, blank examinations were continued to check the possibility of sorption occurring on the walls of the bottle use.

## 3. Results and discussion

After characterising the DDAB/Pmc composite as an adsorbent to determine its capabilities, the retention behaviour of Cr(VI) was calculated using the batch technique. First, different operational factors that impact the adsorption competence were considered. Next, the adsorption method was analysed using diverse isothermal and kinetic forms to obtain data.

### 3.1. Composite characterisation

Several analytical techniques were employed to thoroughly characterise the modified pumice (DDAB/Pmc composite). FTIR spectroscopy was used to identify and confirm the presence of functional groups that play a crucial role in adsorption. XRD analysis provided insights into the crystalline structure and any structural modifications resulting from the treatment process, which can influence material stability. TGA was utilised to assess the thermal stability and decomposition behaviour of the material, ensuring its suitability for practical applications. SEM imaging was conducted to examine surface morphology and detect changes in texture that may affect adsorption efficiency. Lastly, BET analysis was performed to determine the specific surface area and porosity, which are key factors in optimising adsorption capacity.

#### 3.1.1. Characterisation of $H_2SO_4$ activated-pumice and DDAB/Pmc composite

Based on the experimental results of some researchers, it has been shown that there was a growth in sorption efficacy using pumice modified via immersion in strong acids compared to natural, unmodified pumice [39]. All chemical treatments with oxidising

agents used to produce acidic functional groups accompany a decrease in external surface area and whole pore volume, mostly owing to the obliteration of the porous constructions inside adsorbents throughout the oxidative step. Moreover, drenched sorbent in an acidic solution can melt the adulteration compounds (organic content) on the surface of the adsorbent's holes (pores), increasing the adsorbents' surface area and retention capacity. While strong acid activation reduced the organoimpurities of the sorbent and improved surface properties (porosity), surfaces become positively demonstrative with $H^+$, facilitating a further increase in adsorption in the case of negative ions [39,40]. Acid activating a solid is a simple and very effective method to modify the solid surface area, reactivity, homogenisation, and adsorption. This activation results in eradicating exchangeable species. Changes in the physicochemical features of a solid via acid activation can generate many of its interesting and required properties [40]. Also, a grouping of acidly-activation through surfactant (alkyl-ammonium intercalation) offers possible enrichments of solid sorbent possessions. Sulfuric acid is one of the best acids used in activation [39–41].

This section offers some physical and chemical features of $H_2SO_4$ pumice and synthetic DDAB/Pmc composite. The elemental composition of the DDAB/Pmc composite was investigated using EDX analysis. A separate peak consistent with the constituent elements (Si, Al, Ca, O, S, C) was observable, besides peaks consistent with additional elements, such as Ti and Fe. Further elements with a percentage abundance under 1% can be presumed as micro-components, Figure S1 in supplementary file.

***3.1.1.1. SEM study.*** SEM was applied to predestine the $H_2SO_4$ activated-pumice and organo-modified $H_2SO_4$ activated-pumice (DDAB/Pmc) morphology and micro-graphs displayed in Figure S2. Images (Figure S2A, C, E) of $H_2SO_4$ activated-pumice point out that the $H_2SO_4$ activated surface had a porous surfaces. The SEM images of organo-modified activated pumice with a double-chain cationic surfactant (DDAB/Pmc) are specified in Figure S2 (B, D, F). As is seen in this figure, the exteriors of $H_2SO_4$ activated-pumice particles reformed due to organ modification with a surfactant, and the porous system could not be visible. After the organ modification reaction, DDAB/Pmc composite surfaces became smoother than those of H2SO4 pumice. DDAB/Pmc Smoother surface may be owed to the sorption of DDAB onto $H_2SO_4$ activated-pumice filling and covering natural cracks and pores, Figure S2 (B, D, F). This is evidence of the success of the organ modification process of $H_2SO_4$ pumice. In other words, the DDAB molecules as monomers were easily retained onto the exterior of the activated stone, owing to the role of the $H_2SO_4$ in emptying the pores and cleaning them of impurities [40].

Such a phenomenon was earlier detected when modifying the original pumice with different organic and inorganic species. In some studies, original pumice stone and composites of $MgCl_2$/pumice and polyacrylonitrile/pumice were used as adsorbents, displaying that this stone had an asymmetrical surface per higher holes and cracks. However, a flatter exterior and fewer cavities and pores were detected after loading and impregnation through $MgCl_2$ and poly-acrylonitrile [34].

***3.1.1.2. $N_2$ Adsorption/desorption isotherm characteristics.*** Adsorption capacity is a throwaway to calculate the volume of N2-gases sorbed at diverse relative pressures, $P/P_o$, where $P$ is the $N_2$-pressure, and $P_o$ is the fullness $N_2$ of DDAB/Pmc composite

(adsorbent). Different instruments give adsorption_isotherm in points by calculating the extent of $N_2$ sorbed besides equilibrium $N_2$-pressure. Desorption_isotherms could be attained via computing $N_2$-amounts detached from DDAB/Pmc composite (adsorbent) with relative $N_2$-pressure dropped.

By observing the shape and knowing the details of the adsorption/desorption isotherm curves, such as the hysteresis loops, we can achieve beneficial data regarding the physiosorption way in DDAB/Pmc pores that could aid qualitatively designating DDAB/Pmc pore styles also shapes [30,42]. $N_2$-isotherms might be gathered in 5 styles (Type 1 to Type 5). Those $N_2$-isotherms aren't commonly reversible or retain and exhibit hysteresis kinks or loops [43]. It is identified that there are open pores, for example, tubular pores, wedge or nail-shaped pores, equivalent plate-pores which opened at both tops or round, especially tinny deadlock-pores, create hysteresis. There are five pore types correlated with hysteresis loops [44].

The $N_2$_isotherm curves and pore-size-distribution diagrams of unchanged-pumice besides the DDAB/Pmc composite are shown in Figure S3 and Figure S4. The natural-pumice and DDAB/Pmc fit to *Type-IV* isotherm with hysteresis-loop (Figure 3(a) andFigure 4(a)) according to the IPUAC classification, which resulted from capillary condensation in the typical mesoporous structure [30,44] (diameter (width), $2 < d < 50$ nm) at wide relative-pressure variety about 0.1–0.9, adsorption line and de-sorption line rapidly jet and coincide at ending. Thus, the amounts of these hysteresis indicate that natural pumice and DDAB/Pmc had a lot of mesopores. Also, these figures display that the natural-pumice and DDAB/Pmc composite had no macro-pores ($d > 50$ nm) and negligible extent of micro-pores ($d < 2$ nm), Figure S3b and Figure S4b.

The IUPAC categorised hysteresis into 4 sorts, demonstrating an unalike pore profile or shape. Type-*H1* typifies cylindrical or tubular pore wholes in which both trimmings are uncluttered and capillary (tube) condensation happens in mid of relative pressure; Type-*H2* is correlated through ink-bottle-shaped pore aggregates with openings (pores) connectivity and rough pores structures, *H3* forms are credited to wedge-formed openings moulded via moveable stacking of scaly units, and the last one, Category *H4* loops are consequence of slit-shaped openings resultant as of inside equivalent pore structures in rock [43,44].

Accordingly, hysteresis loops of the natural pumice and DDAB/Pmc belong to Type H4, viewing that the natural pumice and DDAB/Pmc have several allocations of opening types or forms and pore distance that typically stem to slit approximating openings and 2 aligned platter fissures. Type *H4* indicates that the adsorbent's pore shapes remain open, and open slit-alike openings (pore styles) in equivalent platter construction are paramount pore styles [42–44]. Besides, from Figure 3Sb and Figure 4Sb, the pore size distribution is chiefly concentrated between about 2–8 nm and 3.5–10 nm for natural pumice and DDAB/Pmc, respectively, which is produced by the cavities formed through the freezing of the original pumice stone, which is compatible with the SEM.

$S_{BET}$ of ordinary-pumice and DDAB/Pmc composite was notable regarding the BET performance. It revealed a meaningfully higher $S_{BET}$ for the DDAB/Pmc composite if equated to a regular one, 93.422 $m^2.g^{-1}$ and 17.313 $m^2.g^{-1}$ correspondingly. $S_{BET}$ of DDAB/Pmc composite was enriched (about 6 terms of natural-pumice value). Large reasonable $S_{BET}$ of the DDAB/Pmc owed to the elimination of constituents or impurities that occupy the openings of natural pumice by $H_2SO_4$ in the activation step, which results

in easier access to the surface and, thus, a larger surface area. This is identical to what was obtained using the SEM analysis previously. The extended pore volume and pore diameter of DDAB/Pmc with our modification that results in improved surface area have been reported by other researchers [34,40]. This shows the important role of the activation step with 5 M sulphuric acid. $S_{BET}$ of DDAB/Pmc is 93.422 $m^2.g^{-1}$, larger than the surface area of many sophisticated adsorbents, making this prepared composite suitable for application in wastewater treatment operations.

***3.1.1.3. FTIR study.*** Figure 1 depicts the FT-IR spectra of natural pumice (a) and $H_2SO_4$ pumice (b) at wavelengths 400–4000 $cm^{-1}$. According to what is shown in Figure 1(a), it could be seen that peak near 1793 $cm^{-1}$ attributed to H – O – H bond bending vibration [45,46]. Peak around 1406 $cm^{-1}$ is assigned to distortion vibration of – OH groups (maybe Al – and/or Si-OH distortion vibration) [46]. A peak of ~871 *1/cm* can be assigned to bending vibrations of Si – O – Si [47]. The stretching vibration of Al – O – Si was verified near ~711 *1/cm* [45]. Bending modes of Al – O and Si – O links were observed between 400 and 500 $cm^{-1}$ [45]. In general, the spectrum of natural pumice unmodified in any way was observed to be very similar and in good agreement with those results previously reported and published in the literature [45,47].

The FTIR spectrum of $H_2SO_4$ activated pumice is illustrated in Figure 1(b). From this figure, it could be seen that the peaks characteristic to the natural pumice (426, 443, 711, and 871 $cm^{-1}$) but at different positions (418, 424, 657 $cm^{-1}$), whereas peak observed on ~871 *1/cm* was missing. Peaks displayed by 596, 1006, and 1082 corresponded to asymmetric bend, symmetric stretch, and asymmetric stretch of sulphate anion, respectively [48]. The peak at ~1618 1/cm could be assigned to the winding vibration of the H – O – H bond [45,46]. Two peaks through 3604 and 3547 *1/cm* attributed to $H_2O$ stretching shaking (moisture) in the matrix and – OH sets [45].

FTIR spectrum of the DDAB/Pmc composite is illustrated in Figure 1(c). From this figure; it could be seen that the peaks characteristic to the $H_2SO_4$ activated pumice in addition to three peaks that corresponded to the organic DDAB (1683, 2855, and 2926 $cm^{-1}$). Peak on 1683 $cm^{-1}$ is probably C = N stretching mode [49]. Peaks that become apparent at 2855 cm than 2926 $cm^{-1}$ may be due to the symmetric and asymmetric widening vibrations of methylene in DDAB [50].

Figure 1(c,d) depicts FT-IR spectrums for DDAB/Pmc and Cr(VI)-loaded DDAB/Pmc (before and after loading with Cr(VI) ions). According to what is shown in Figure 1, there is almost no change (shifts) in the peak position after Cr (VI) loading. This result confirmed that no function group is consumed in this adsorption process. On the other hand, the new bands at 792 and 937 $cm^{-1}$ in the Cr(VI)-loaded DDAB/Pmc could be due to Cr – O – Cr and Cr – $O_3$, respectively [51], and hence we can predict that this sorption controlled with physical sorption. Generally, very slight shifts were observed for some vibrations. The presence of these vibrations with minor shifts in DDAB/Pmc composite loaded with Cr(VI) anions ensures the association of DDAB molecules with the Cr(VI). Generally, the FTIR spectra of the original and modified pumice samples seemed approximately identical and compatible with those described in the literature [34].

***3.1.1.4. Thermogravimetric study.*** The thermal decomposition features of DDAB/Pmc composite were studied at a constant proportion (10°C/min) from 28°C to 600°C. TG/

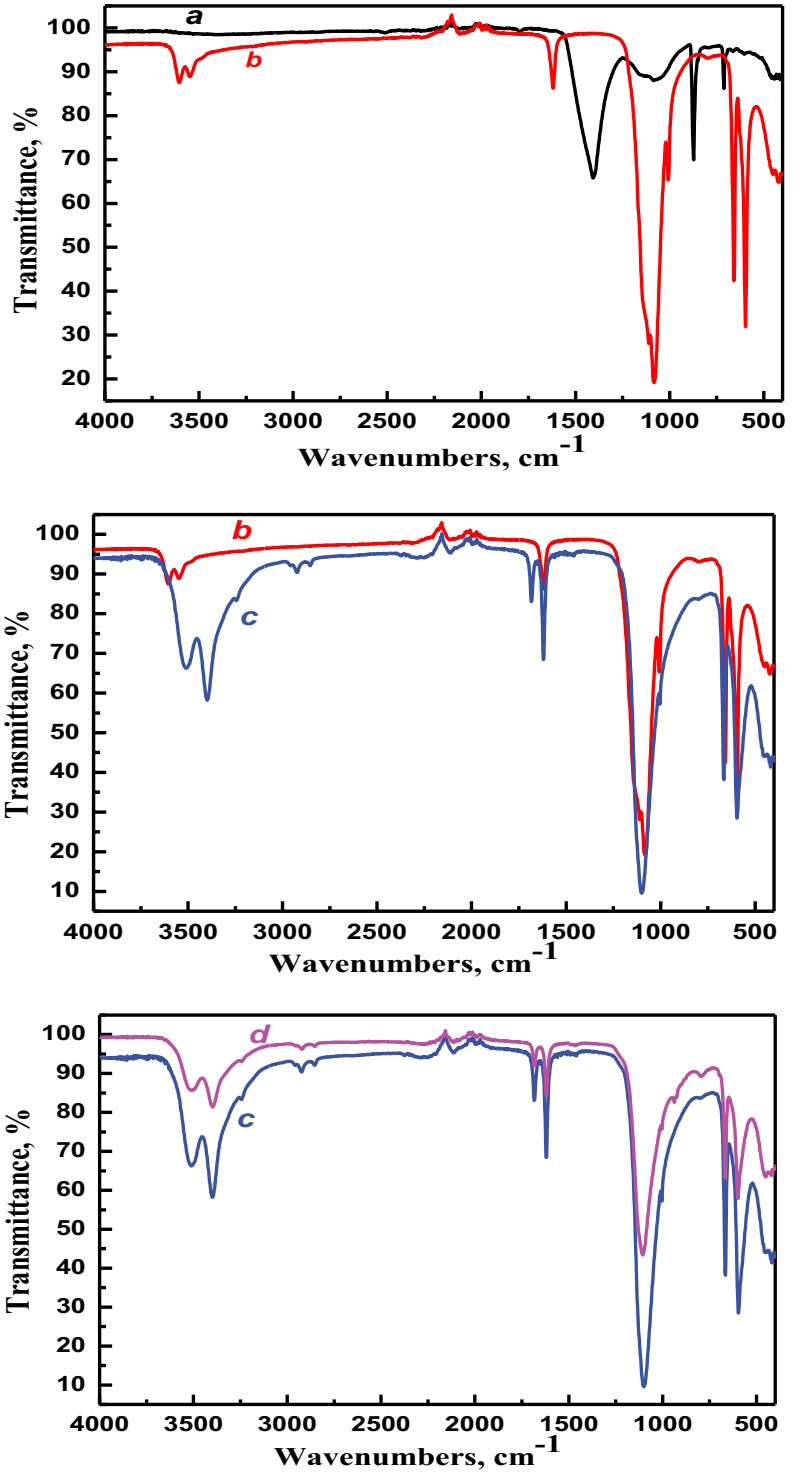


**Figure 1.** The FTIR spectra of (a) natural pumice, (b) $H_2SO_4$ activated-pumice, (c) DDAB/Pmc and (d) Cr(VI)-loaded DDAB/Pmc.

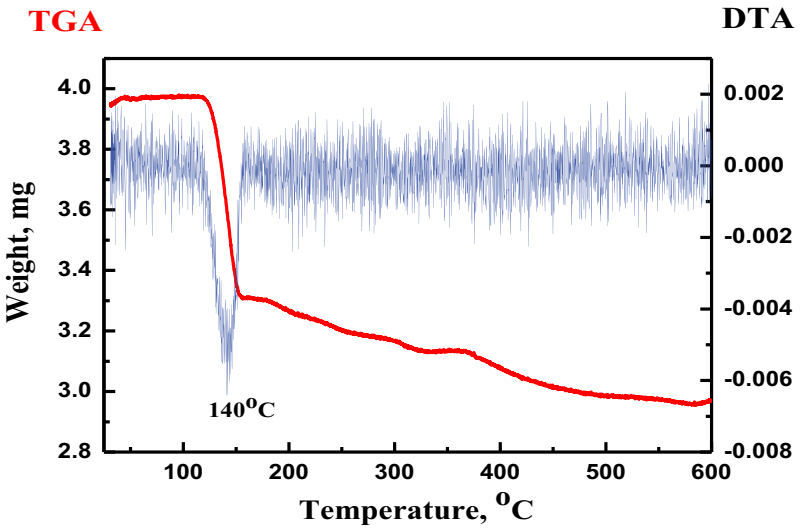


**Figure 2.** Thermogravimetric (TG) and differential thermal (DTA) analyses curves of DDAB/Pmc composite.

DTA curve DDAB/Pmc is shown in Figure 2. A sharp weight loss of about 16.72% was observed between 120°C and 155°C, possibly due to the loss of physical adsorbed water present [52] as confirmed by the endothermic peak of the DTA curve at 140°-C. A sluggish loss of about 5.23% on warming to about 367°C might be owed to the complete decomposition of DDAB [53]. Extra mass (~5.36%) damaged amongst 367–600°C may be owed to intensification or condensation of interstitial $H_2O$ molecules [52]

***3.1.1.5. X-ray diffraction (XRD) studies.*** XRD spectra obtained for natural pumice, DDAB/Pmc composite, and Cr(VI)-loaded DDAB/Pmc are gotten in Figure 3. According to what is exposed in Figure 3(a), it could be realised that the results of the XRD pattern of natural-pumice stone demonstrated that the highest constituent of this stone was silicon dioxide ($SiO_2$: quartz), with major greatness peaks linked to silicon dioxide ($SiO_2$) at $2\theta = 26.05$, 30.08, 50.22 and 55.50° [52]. The crystallite length ($D$) was computed via Debye-Scherer's formal [52].

$$D = \frac{0.9\lambda}{\beta \cos\theta},$$

where λ (λ = 1.5406 Å), β and θ are beam wavelength, full-width-at-half-maximum (FWHM) of intense peak and Braggs-angle, respectively. Found on exceeding calculation, D of natural-pumice computed −1. The most intense peak at 30.08 degrees (2θ) was 15 nm. Figure 3(b) depicts the XRD pattern of the DDAB/Pmc composite. From Figure 3(b), it could be seen that the degree of crystallinity was decreased, and the peaks' positions were changed after the organo-modification with amorphous DDAB molecules. In addition, the crystallite size of the natural pumice was reduced to 13.9 nm after the organo-modification process. The XRD pattern of Cr(VI)-loaded DDAB/Pmc is seen in Figure 3(c),

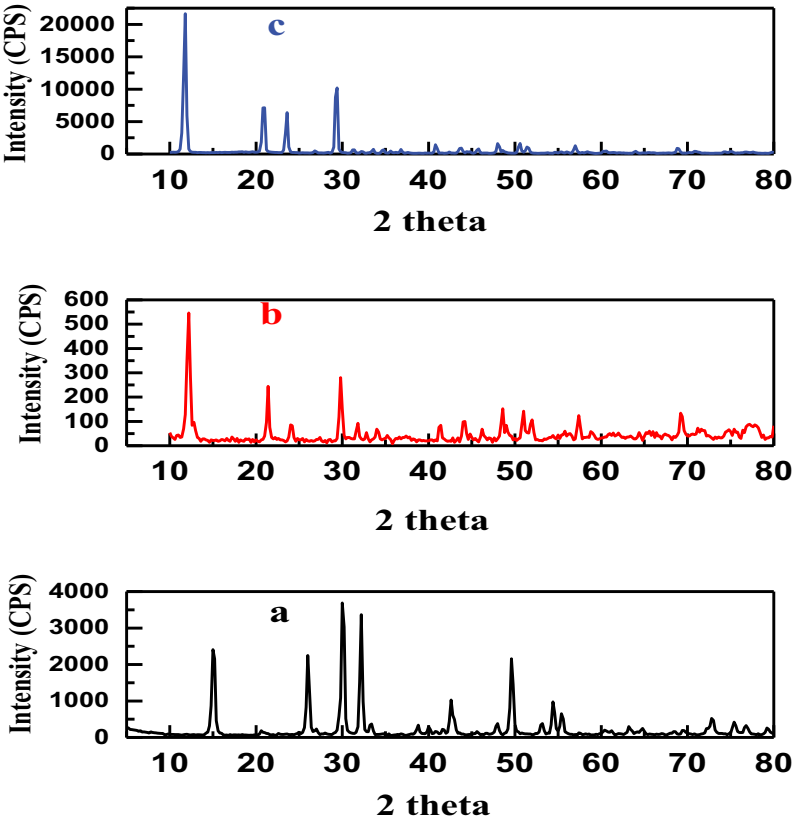


**Figure 3.** XRD patterns of (a) natural pumice, (b) DDAB/Pmc, and (c) Cr(VI)-loaded DDAB/Pmc.

and a striking feature in this chart is the upward surge in the intensity of the peaks. Also, many peaks disappeared, and the positions of the other peaks changed. These changes are evidence of Cr(VI) ions adsorption.

## 3.2. Performance of adsorption

### 3.2.1. Effect of pH

Values of pHs in any solutions are deliberated to have power on exterior charge for any sorbent such as DDAB/Pmc, the ionisation and speciation of adsorbate such as Cr(VI) oxyanions in solution [20,21]. Potassium-dichromate ($K_2Cr_2O_7$) liquefies in $H_2O$ and disassociates into dichromate ions that extra disassociate towards $HCrO_4^-$or $CrO_4^{2-}$ dependent on pH and chromium extent. Researchers often discuss the presence of only $CrO_4^{2-}$ and $Cr_2O_7^{2-}$ in the Cr(VI) solution. Nevertheless, the reality of supplementary sorts correspondingly been established: hydrogen-chromate or bi-chromate ($HCrO_4^-$), chromic-acid ($H_2CrO_4$), hydrogen di-chromate ($HCr_2O_7^-$), tri-chromate ($Cr_3O_{10}^{2-}$), and tetra-chromate ($Cr_4O_{13}^{2-}$). Whereas $H_2CrO_4$, $HCr_2O_7^-$, $Cr_3O_{10}^{2-}$ or $Cr_4O_{13}2^-$ are only formed in exciting conditions, at great acidity and a huge concentration of chromate anions [22]. Figure 4 illustrates Cr + 6 aqueous anions as a sense of pH values considered by HYDRA.MEDUSA [20] chemical equilibrium toll (soft-ware) on [Cr(VI)] = 100 mg.$L^{-1}$, room temperature and pH range

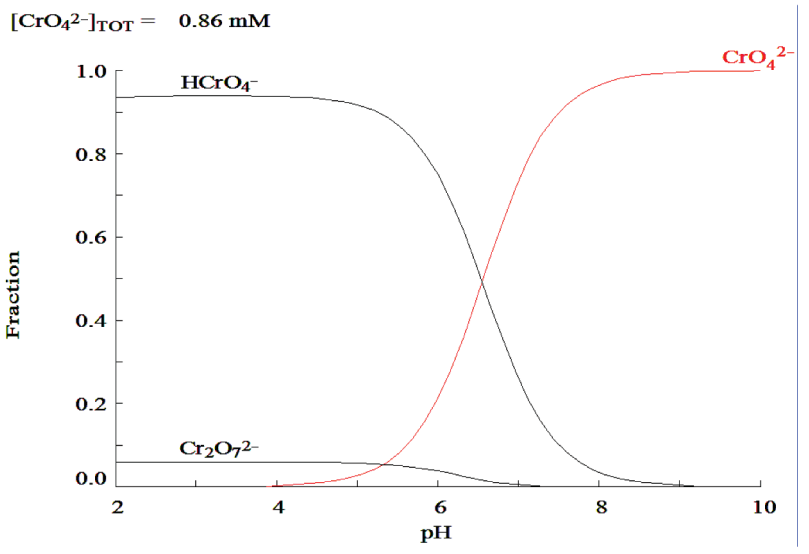


**Figure 4.** Speciation of Cr(VI) in solution with different pH values.

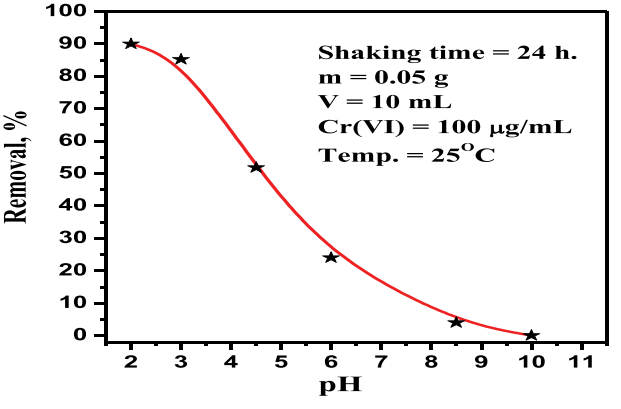


**Figure 5.** Effect of pH on adsorption of Cr(VI) onto DDAB/Pmc.

2.0–10.0. Cr(VI) happens in $H_2O$ through unlike speciation, in pH range of 2–6, the major form is $Cr_2O_7^{2-}$ and $HCrO_4^-$, at pH greater or nearer to 6 the chromium species exists in the form of $CrO_4^{2-}$ and the affinity of this anion is very low in comparison with $Cr_2O_7^{2-}$ and $HCrO_4^-$, Figure 4.

It can be apparent visibly that pH values rule sorption through Figure 5. The best removal % condition was pH 2, reaching a maximum rate of 90%. A general decrease in % *R* with growing pHs is supposed. At high pH values, the plentiful hydroxyl sets, $OH^-$, are dominated by anions of Cr(VI) to seize adsorption active sites, and thus, a low % R of Cr(VI) is obtained. The sum of OH- converts to smaller and %R growths through decreasing pH. According to the texts [23], sorption of any metal ions on inferior pH values habitually goes to outer-sphere-surface complexation. Besides, as developed, Cr(VI) elimination happens by acidic pHs, and subsequently, existent Cr(VI) wastewaters are acid by nature;

there is no necessity for pH adjustment for practical applications of DDAB/Pmc composite under consideration. Where the engineering sewages are tannery waste (near pH 2), electro-plating waste (around pH 2.2), and Cr-plating discharge (pH 1) [24]. Comparable discovery proceeding pH tendency has been stated in Cr(VI)-oxyanions sorption of training by earlier academics [25,26].

Further removal at acidic pH designates that lower pHs lead to a growth in[$H^+$] ions on the exterior of the DDAB/Pmc composite, resulting in a considerably strong electrostatic attraction among the positively charged DDAB/Pmc composite surfaces and the chromate species. Lower *R*% of Cr(VI) at extreme pH values could be due to twin opposition of $OH^-$ and Cr(VI) anions to be sorbed onto the exterior of DDAB/Pmc, which groups of $OH^-$ dominate. Satisfactory results at small pHs can be thanks to the neutralisation of charges (negative) on the exterior of DDAB/Pmc by extra $H^+$, thereby simplifying the dispersal of $Cr_2O_7^{2-}$ and $HCrO_4^-$ and its following adsorption, as $Cr_2O_7^{2-}$ and $HCrO_4^-$ are the main anionic species of Cr (VI) at lower pH, Figure 5. Consequently, it originated from the subtraction of Cr(VI) oxyanions from observations, and a pH of 2 was considered its top pH for supplementary investigational studies.

### 3.2.2. *Influence of contact time*

Contact time is crucial in wastewater treatment, as faster adsorption indicates higher efficiency [24]. For Cr(VI) removal using DDAB/Pmc, equilibrium was achieved within 5 to 180 minutes, demonstrating its effectiveness, Figure 6.

The outcomes in Figure 6 specified that sorption grows abruptly at the initial period and steadily smoothies into equilibrium. So, it can be supposed that adsorption occurred in two stages: first quick step followed by the second slower phase till equilibrium was reached. The adsorption processes reach equilibrium after 60 min; therefore, the contact time for further studies is fixed to 60 min. The high *R* % at the initial period can be owing to the fact that all active sorption seats were originally unused of composite for % Cr

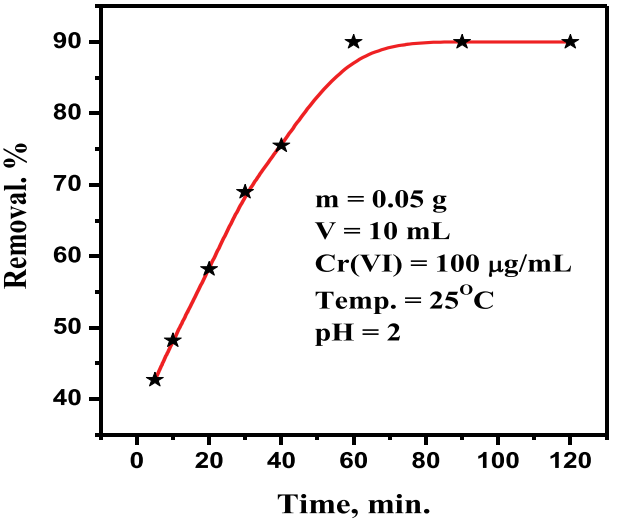


**Figure 6.** Effect of contact time on the adsorption of Cr(VI)onto DDAB/Pmc.

anionic abstraction, and [Cr(VI)] species gradient in the first portions of the medium was great. Earlier, Cr(VI) removal via composite lessened meaningfully, owing to diminishing the sum of sorption active sites, electro-static prevention instigated by previously eliminated species, and gentle pore-diffusion of Cr(VI) species [24,26]. Next, enlarged time, the residual vacant surface active sites are difficult to employ owing to repulsive forces among Cr(VI) species onto DDAB/Pmc and aqueous [20,26].

### 3.2.3. Effect of composite amount

The influence of diverse doses of DDAB/Pmc on the elimination of 100 µg/mL Cr(VI) was passed obtainable, and data were displayed in Figure 7. DDAB/Pmc amount ranged from 0.01 to 0.05 g; however, wholly, other parameters were retained as constant as acidity, contact time, sample size, and temperature were kept constant.

The observations disclose that an increase in the removal efficiency of Cr(VI) happens with the consistent growth in DDAB/Pmc quantity. The growth in abstraction efficacy per simultaneous growth in the DDAB/Pmc measure is due to increased surface area and more active functional sets. Therefore, additional active places were obtainable for the sorption of Cr(VI) species [3,4]. It can be seen from Figure 7 that when the DDAB/Pmc dose is bigger (from 0.01 g to 0.05 g), abstraction efficacy is bigger, starting from 20% to 90%.

### 3.2.4. Influence of Cr(VI) concentration

Figure 8 explores the impact of the initial Cr(VI) species concentration (10–100 µg/mL) on adsorption on DDAB/Pmc.

The capacity values at equilibrium, $q_e$, are bigger with a rise in initial [Cr(VI)]. Cr(VI) species stay sorbed by specific DDAB/Pmc composite locations. In contrast, per growing [Cr(VI)], the specific locations are saturated, and active locations, owing to the extreme exterior area of DDAB/Pmc, are occupied. Ordinarily, adsorption capacities ($q_e$) increase with the increase in [Cr(VI)]. This might be because growths in the initial [Cr(VI)] augment the interface amongst the Cr(VI) species and the DDAB/Pmc surface of the composite [19].

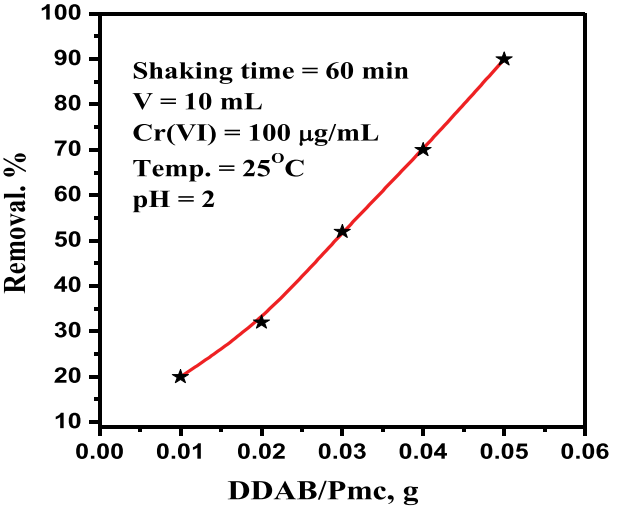


**Figure 7.** Effect of DDAB/Pmc amount on the adsorption of Cr(VI).

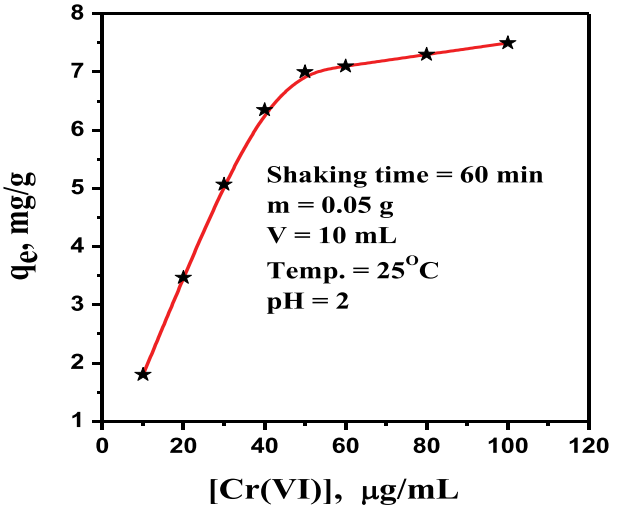


**Figure 8.** Effect of initial Cr(VI) concentrations on the adsorption of Cr(VI).

The initial concentrations of anion species offer a significant driving strength to restrain altogether mass-transfer oppositions of the anion species amongst bulk solution and DDAB/Pmc. Hereafter, higher initial [Cr(VI)] anions' willpower enriches the adsorption procedure [20,26].

### 3.3. Adsorption molding

Isotherm models like Langmuir and Freundlich help analyse adsorption mechanisms, with Langmuir assuming monolayer adsorption and Freundlich describing multilayer adsorption. Kinetic models, including pseudo-first-order (physisorption) and pseudo-second-order (chemisorption), are crucial for understanding adsorption rates and optimising adsorbents for pollutant removal [54,55].

#### 3.3.1. Adsorption kinetic

Adsorption kinetics studies are crucial for understanding the removal mechanism and optimising batch treatment systems [32]. Experimental kinetic data of Cr (VI) anions, computed from equations number (4, 5, and 6), was correlated through kinetics models: PFO, PSO and IPD models. The linear fitting curves are exposed in Figure 9. In contrast, the calculated values of kinetic parameters of 3 kinetics equations through $R^2$ at diverse temperatures and experimental and theoretical capacities are recorded in Table 1.

It was evident that $q_{cal}$ rates valued by the PFO equation fluctuate considerably from those computed experimentally, telling that sorption of Cr(V) species is not a PFO reaction (Table 1).

Also shown in Table 2, the PSO was found to fit the experimental results of Cr(V) species sorption compared to the PFO, in which relevant values of $R^2$ have been labelled. Additionally, $q_{cal}$ (theoretical values) indicated via PSO plot agree fit to investigational rates. Consequently, it could be established that PSO could be practical in describing the Cr(VI) sorption mechanism onto DDAB/Pmc [29,30]. Thus, in the current case, sorptive

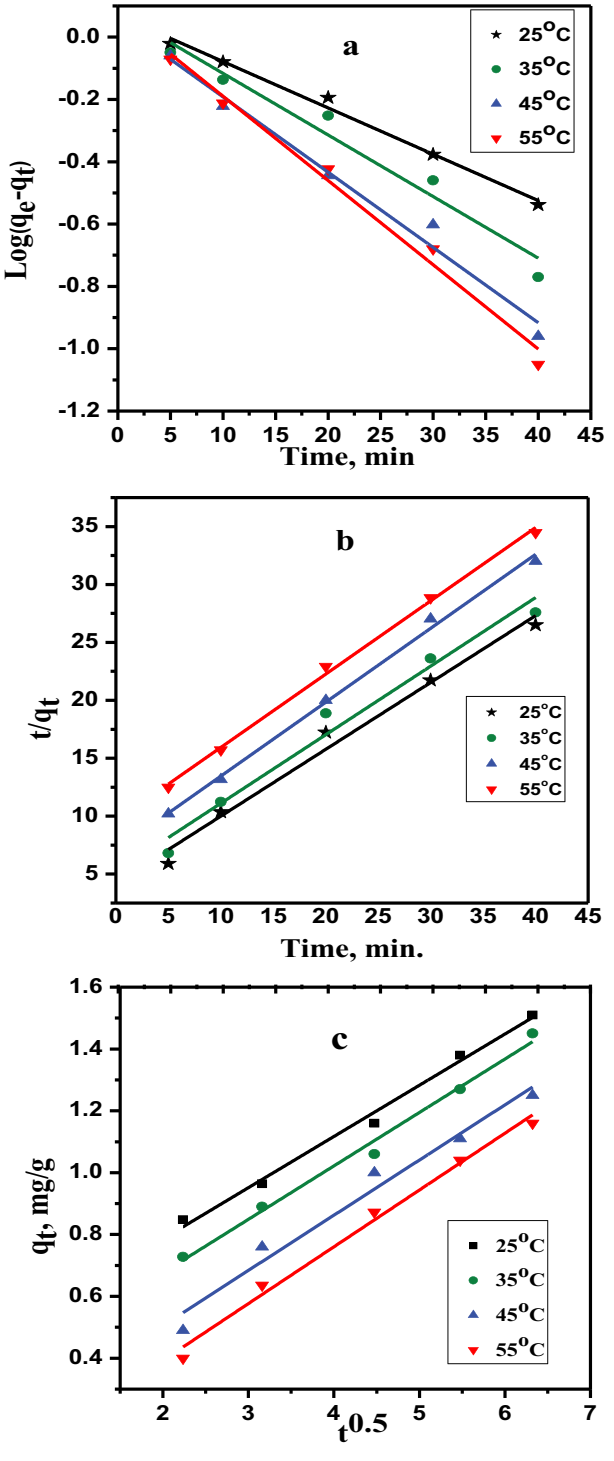


**Figure 9.** Pseudo first-order (a), pseudo second-order (b) and intraparticle diffusion (c) kinetic plots for adsorption of Cr(VI).

**Table 1.** The calculated parameters of the pseudo first-order, pseudo second-order and intra particle diffusion kinetic models of Cr (VI) adsorption onto DDAB/Pmc.

| | | Temperature | | | |
|---|---|---|---|---|---|
| Models | Parameters | 298 K | 208K | 318 K | 328 K |
| Experimental data | $q_{e,exp.}$ *mg/g* | 1.80 | 1.62 | 1.36 | 1.25 |
| First-order kinetic | $k_1$, min.$^{-1}$ | 0.035 | 0.046 | 0.055 | 0.065 |
| | $q_{e,calc}$,mg/g | 1.176 | 1.205 | 1.122 | 1.205 |
| | $R^2$ | 0.991 | 0.995 | 0.991 | 0.988 |
| Second-order kinetic | $K_2$, g/mg.min | 0.079 | 0.068 | 0.058 | 0.042 |
| | $q_{e,calc}$,*mg/g* | 1.733 | 1.689 | 1.567 | 1.579 |
| | $R^2$ | 0.984 | 0.967 | 0.995 | 0.997 |
| Intra- particle diffusion | $K_3$, mg/g.min$^{-0.5}$ | 0.167 | 0.173 | 0.179 | 0.184 |
| | $C$ | 0.455 | 0.330 | 0.149 | 0.026 |
| | $R^2$ | 0.993 | 0.992 | 0.974 | 0.990 |

**Table 2.** Langmuir and Freundlich adsorption isotherm constants for adsorption of Cr(VI) onto DDAB/Pmc.

| Model | Parameters | Value |
|---|---|---|
| Langmuir model | $Q_{max}$, mg/g | 7.810 |
| | $b$, L/g | 0.363 |
| | $R_L$ | 0.216 |
| | $R^2$ | 0.999 |
| Freundlish model | *1/n* | 0.316 |
| | $K_f$, (mg/g)(L/mg)$^{1/n}$ | 2.512 |
| | $R^2$ | 0.7922 |

removal of Cr(VI) onto DDAB/Pmc was found to follow PSO, which counts on the statement that chemisorption or chemical adsorption is the rate key step. Within chemical sorption, Cr(VI) species capacity should stay relational to active sites sum occupied onto DDAB/Pmc exterior [30].

The IPD variables were computed as Weber and Morris informed us. It is verified that the IPD isn't an individual rate-determining step in Cr(VI) sorption, while a substantial contribution in the rate determined via boundary layer diffusion is proposed. The intercept rate is comparable to the range of the boundary layer thickness. It means that Cr(VI) anions are attained at the outside surface of DDAB/Pmc at a moderately high speed, then diffused and bound gradually into the inner DDAB/Pmc surface [30]. These conclusions specified that eliminating Cr(VI) species onto DDAB/Pmc involved more than one process, and IPD isn't rated. They are limiting periods. Such a result is comparable to earlier works [30].

### *3.3.2. Adsorption isotherms*

Adsorption equilibrium provides essential physical and chemical insights for evaluating the efficiency of the removal process. Analysing isotherm data helps derive equations that accurately describe adsorption behaviour for practical applications [32]. The experimental

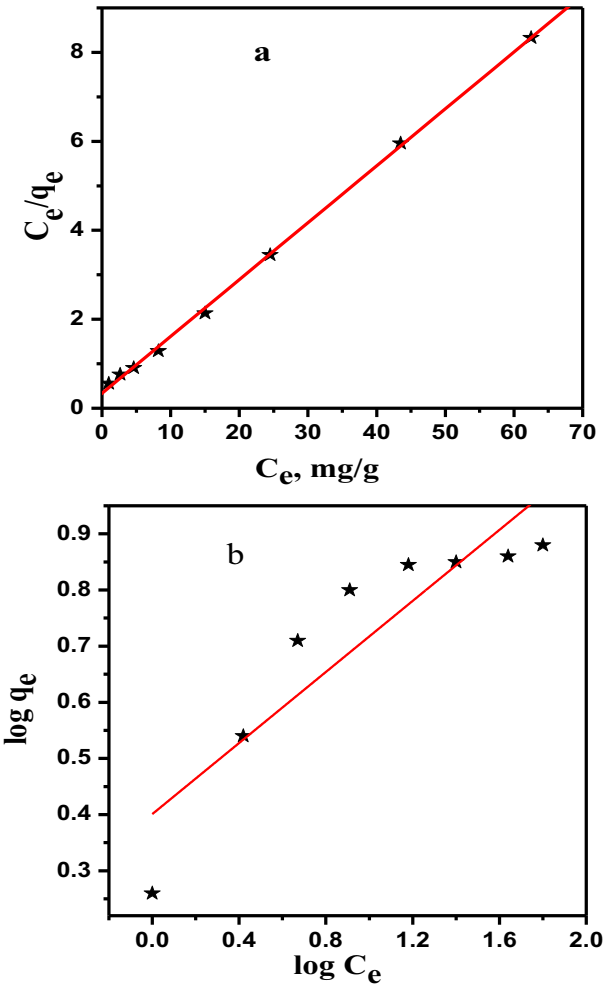


**Figure 10.** Langmuir (a) and Freundlich (b) isotherm plots for adsorption of Cr(VI).

adsorption isotherms of Cr (VI) onto DDAB/Pmc are designed in Figure 10. Parameters besides correlation coefficients ($R^2$) for the abovementioned isotherms exist in Table 2.

The gained investigational equilibrium sorption records were fitted through the mentioned models via equations 7 and 9. Table 2 displays that the Langmuir formula provides the greatest fittings ($R^2 = 0.999$). This suggests that sorption is restricted to mono-layer coverage and that the DDAB/Pmc exterior is moderately similar. $Q_{max}$ computed from linear Langmuir plot was 7.81 mg.g$^{-1}$, similar to the sorption capacities of numerous sorbents [1,3,5,7,31]. The large value of b (the constant associated with the adsorption energy) indicates a strong bonding between Cr(VI) and DDAB/Pmc. The $R_L$ value for adsorption of Cr(VI) on DDAB/Pmc is revealed in Table 2. It specifies very auspicious adsorption ($0.0 < R_L < 1.0$) [30]. Table 2 shows that the Freundlich constant obtained for the current system specifies appropriate adsorption, as it is higher than 1 [30].

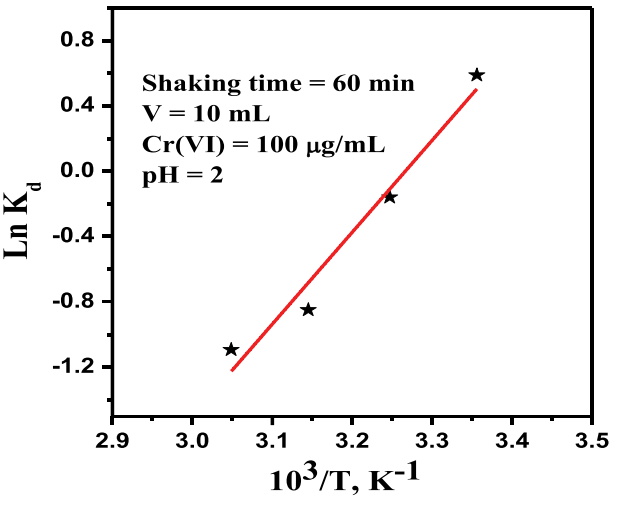


**Figure 11.** Van't Hoff plot for the adsorption of Cr(VI)onto DDAB/Pmc.

### *3.3.3. Thermodynamic studies*

*ΔG°* is a central measure of spontaneity. Removals happen spontaneously at exact some temperatures if *ΔG°* is present at negative rates. Thermodynamic factors (*ΔG°*, *ΔH°*, *ΔS°*) were estimated through equations 10 and 12 via data gotten at temperatures range working (298–328 *Kelvin*). *ΔH°*, *ΔS°* amounts were obtained from the slope and intercept of can't-Hoff-plot of $lnK_c$ *vs. 1/T*, respectively, Figure 11.

The computed parameters for Cr(VI) anions are signified in Table 3. Gibbs free energy of change is utilised to estimate the spontaneity and probability of adsorption processes. A negative *ΔG°* value confirms a spontaneous adsorption process. In contrast, a positive *ΔG°* value suggests a non-spontaneous adsorption process, Table 3. Negative *ΔG°* sign-post spontaneous removal environment of chromate species via DDAB/Pmc considered. *ΔG°* values were found to increase from – 1.457 to 2.98 kJ/mol. The increase in *ΔG°* standards with progress in temperatures directs that the removal procedure of Cr(VI) species on DDAB/Pmc develops extra favourable at lower temperatures. Positive ΔG° values similarly demonstrate that there is an energy barrier. Once Cr(VI) ions arrive from the solution to the particle exterior, certain of the $H_2O$ starting hydration film of ions are stripped off, and the parallel degree-of-freedom of ions is reduced [33]. The analogous phenomenon has been stated for the adsorptive removal of nitrate and nitrite anions [32,33]. Positive *ΔH°* displays that the sorption procedure was endo-thermic. In contrast,

**Table 3.** Thermodynamic parameters for adsorption of Cr(VI) onto DDAB/Pmc.

| Temp, K | ΔH, kJ/mol | ΔS, J/mol.K | ΔG, kJ/mol |
|---|---|---|---|
| 298 | 46.783 | 152.80 | –1.457 |
| 308 | | | 0.410 |
| 318 | | | 2.247 |
| 328 | | | 2.981 |

positive $\Delta S°$ reflects the affinity of the DDAB/Pmc composite for the Cr(VI) anions and suggests some structural changes in Cr(VI) anions and DDAB/Pmc [30,31].

### 3.4. Mechanism of Cr(VI) adsorption

From the results obtained above, we note that negative chromium(VI) sorption decreases continuously with the pH growth. It was also noted that extreme sorption is at pH = 2.0. It is known that chromium exists in different oxidation states, as in Figure 4. The strength of these forms is needful on system pH and balance amongst the unlike ionic types of Cr(VI), like so [56]:

$$H_2CrO_4 \leftrightarrow H^+ + HCrO_4 \tag{13}$$

$$HCrO_4^- \leftrightarrow H^+ + CrO_4^{2} \tag{14}$$

$$2HCrO_4^- \leftrightarrow Cr_2O_7^{2-} + H_2O \tag{15}$$

Therefore, the significantly rapid decrease in the removal of these negative ions of chromium(VI) through increasing pH might be owed to the statement that diminution in pH or the increase in the acidity of the medium generates growth in protonated groups and $H^+$ on DDAB/Pmc composite exterior, which causes a meaningfully strong attraction (electrostatically) amongst $HCrO_4^-$ (species is abundant at these conditions) and the positively charged DDAB/Pmc composite surface. This finding displays that the chief mechanism of Cr(VI) adsorptive removal on DDAB/Pmc composite is via contact amongst Cr(VI) and groups (protonated) of DDAB/Pmc composite surface.

In another way, it is well identified that $HCrO_4^-$ and $Cr_2O_7^{2-}$ species accounted for nearly 80% besides 20%, correspondingly, in the pH range from 2.0 to around 5.0, Figure 4. In the many real industrial wastewaters at pH 2.2, $HCrO_4^-$ and $Cr_2O_7^{2-}$ species were the principal species. Since the DDAB/Pmc composite (aminated pumice) was positively charged in the pH 2.0–5.0 range, especially by pH of 2, protonated function groups such as amine groups would adsorb anionic $HCrO_4^-$ and $Cr_2O_7^{2-}$ through electrostatic attraction as follows ($-N^+$ and $HCrO_4^-$ as representatives). In the FTIR spectrum of the DDAB/Pmc composite after Cr(VI) adsorption, the minor shifts of some vibrations verified the involvement of protonated groups in chromate removal, Figure 1.

$$N^+ + HCrO_4 - \rightarrow -N^{+}\cdots HCrO_4^- \tag{16}$$

$$-H^+ + HCrO_4 - \rightarrow -H^{+}\cdots HCrO_4 \tag{17}$$

$$-H_2^+ + HCrO_4^- \rightarrow -H_2^{+}\cdots HCrO_4^- \tag{18}$$

### 3.5. Comparison of $Q_{max}$ for several adsorbents

The adsorption capacity ($Q_{max}$) of DDAB/Pmc was compared with other adsorbents, showing its strong potential for Cr(VI) removal. Results indicate that DDAB/Pmc outperforms or rivals several low-cost adsorbents previously recommended for decontamination, Table 4.

**Table 4.** Comparison of adsorption capacities of various adsorbents for Cr(VI).

| Adsorbent | $Q_{max}$, mg/g | References |
|---|---|---|
| Fe@PACB-700 | 22.24 | [35] |
| Nanolignin | 30.94 | [36] |
| Tella residue | 15.60 | [37] |
| Pisum sativum seed shell | 8.50 | [37] |
| Magnetic Zn/Iron-based sludge/biochar composite | 27.04 | [38] |
| Methylated biomass of Spirulina platensis | 16.70 | [57] |
| Activated carbon of Leucaena leucocephala | 13.85 | [58] |
| Montmorillonite magnetite nanoparticles | 10.60 | [59] |
| Waste activated carbons treated with sulfuric acid | 7.490 | [60] |
| DDAB/Pmc composite | 7.810 | This study |
| Untreated papaya peel | 7.160 | [61] |
| Rubber wood sawdust | 4.87 | [62] |

### *3.5.1. Conclusion*

This research presents a practical method for purifying polluted water and wastewater by removing Cr(VI) through adsorption using widely available and cost-effective materials. Treating pumice with 5 M $H_2SO_4$ significantly enhances its porosity, surface area, and acidic properties, leading to improved adsorption performance. Additionally, modifying the acid-treated pumice with a cationic surfactant (DDAB) resulted in an efficient adsorbent composite. The adsorption behaviour Experimental results demonstrated that the adsorption process occurs rapidly, reaching peak efficiency within 60 minutes at pH 2 for Cr(VI) anions. The removal mechanism aligned well with the Langmuir isotherm model, indicating a maximum adsorption capacity of 7.81 mg/g. Moreover, kinetic analysis confirmed that sorption followed a pseudo-second-order model, suggesting a chemisorption-driven interaction The DDAB/Pmc composite is environmentally friendly in nature, as it does not release harmful products. Moreover, its affordability and high efficiency make it a strong candidate for large-scale implementation. The findings from this study offer critical insights for designing an effective and economical treatment system for Cr(VI)-contaminated water and industrial effluents.

## Acknowledgments

The authors acknowledge support from the KIT-Publication Fund of the Karlsruhe Institute of Technology.

## Disclosure statement

No potential conflict of interest was reported by the author(s).

## Funding

This work was funded by the Deanship of Scientific Research at Jouf University under grant No. [DGSSR-2023-02-02320].

## ORCID

AbdElaziz A. Nayl http://orcid.org/0000-0002-0314-3408

## References

[1] S. Singh, S. Das and S. Srivastava, Environ. Technol. Innov. **32**, 103310 (2023). doi:10.1016/j.eti.2023.103310
[2] S.A. Khan, M.F. Siddiqui and T.A. Khan, Sonochem. **60** (104761), 104761 (2020). doi:10.1016/j.ultsonch.2019.104761
[3] O.S. Gonsalves and P.R. Nemade, Chemosphere. **351**, 141246 (2024). doi:10.1016/j.chemosphere.2024.141246
[4] S.A. Khan, D. Hussain, N. Abbasi and T.A. Khan, Chemosphere. **289** (133232), 133232 (2022). doi:10.1016/j.chemosphere.2021.133232
[5] Z. Li, J. Dong, X.F. Fidelis Azi, Z. Ge, Y. Yang, S. Sun, X. Guan, M. Dong and M.-S. Dong, Npj Clean Water. **7** (1), (2024). doi:10.1038/s41545-024-00318-5
[6] Y.A. El Kassimi, R. El Himri, M. El Haddad and M. Laamari, Int. J. Environ. Anal. Chem. **103** (3), 491–513 (2021). doi:10.1080/03067319.2020.1861261
[7] Y.A. El Kassimi, M. El Himri, M.R. Laamari and M. El Haddad, Biointerface. Res. Appl. Chem. **11**, 12662–12679 (2021). doi:10.33263/BRIAC115.1266212679
[8] T.A. Qureshi, T.A. Gadhi, D.A. Khokhar, I.A. Najma, N. Channa, S. Bakhat, T. Rafique and R. Mahar, Minerals. **13**, 1131 (2023). doi:10.3390/min13091131
[9] A. Gupta, S. A. Khan, and T.A. Khan , *Remediation of Textile Wastewater by Ozonation* (Scrivener Publishing LLC, Beverly, MA, 2021). doi:10.1002/9781119818915.ch11
[10] M. Irshad, S. Sattar, R. Nawaz, A. Bukhari, M. Waseem, A. Irfan, A. Inam and M. Zaki, Environ. Saf. **263**, 115231 (2023). doi:10.1016/j.ecoenv.2023.115231
[11] B. Liu, Y. Xin, J. Zou, F.M. Khoso, Y. Liu, X. Jiang, S. Peng and J. Yu, Molecules. **28** (2), 639 (2023). doi:10.3390/molecules28020639
[12] Y.A. El Kassimi, M.E.H. Imane Nadir, R. Laamari and M. El Haddad, Biointerface. Res. Appl. Chem. **12**, 1247 (2022). doi:10.33263/BRIAC121.12471262
[13] O. Kusku, B.L. Rivas, B.F. Urbano, M. Arda, N. Kabay and M. Bryjak, J. Chem. Technol. Biotechnol. **89** (6), 851 (2014). doi:10.1002/jctb.4320
[14] Z. Yao, Y. Li, Y. Cui, M. Zheng, B. Zhu, H. Xu and L. Zhu, Desalination. **355** (91), 91–98 (2015). doi:10.1016/j.desal.2014.10.030
[15] S.M. Çifçi and S. Meriç, Desalin Water. Treat. **57** (39), 18131 (2016). doi:10.1080/19443994.2015.1124348
[16] A.I. Ismail, O.I. El-Shafey, M.H. Amr and M.S. El-Maghraby, Int. Sch. Res. Not. **2014** (1), 1–9 (2014). doi:10.1155/2014/259379
[17] Y.A. El Kassimi, R. El Himri, M. El Haddad and M. Laamari, Int. J. Environ. Anal. Chem. **103** (6), 1223–1244 (2021). doi:10.1080/03067319.2021.1873306
[18] F. Akbal, J. Colloid. Interface Sci. **286** (2), 455 (2005). doi:10.1016/j.jcis.2005.01.036
[19] I.M. Ahmed, R.F. Aglan and M.M. Hamed, J. Radioanal. Nucl. Chem. **314** (3), 2253 (2017). doi:10.1007/s10967-017-5586-2
[20] M. Ahmed, M.M. Hamed and S.S. Metwally, Chin. J. Chem. Eng. **28** (6), 1582 (2020). doi:10.1016/j.cjche.2019.12.027
[21] M.M.S. Ali, E.A. Abdel-Galil and M.M. Hamed, Appl. Radia. Isoto. **166**, 109357 (2020). doi:10.1016/j.apradiso.2020.109357
[22] M. Szabó, J. Kalmár, T. Ditrói, G. Bellér, G. Lente, N. Simic and I. Fábián, Inorg. Chim. Acta. **472**, 295 (2018). doi:10.1016/j.ica.2017.05.038
[23] S.B. Johnson, T.H. Yoon, B.D. Kocar and G.E. Brown, Langmuir. **20** (12), 4996 (2004). doi:10.1021/la036288y
[24] F.B. Ojembarrena, H. Sammaraie, C. Campano, Á. Blanco, N. Merayo and C. Negro, Nanomaterials. **12** (23), 4172 (2022). doi:10.3390/nano12234172

[25] S. Gupta and B.V. Babu, Bioresour. Technol. **100** (23), 5633 (2009). doi:10.1016/j.biortech.2009.06.025
[26] M.M. Hamed, R.S. Hassan and S.S. Metwally, Process Saf. Environ. Protect. **124** (31), 31–38 (2019). doi:10.1016/j.psep.2019.01.033
[27] M.M. Hamed, I.M. Ahmed and M. Holiel, Radiochim. Acta. **107** (12), 1161 (2019). doi:10.1515/ract-2019-0010
[28] B. Adane, K. Siraj and N. Meka, Kinetic, Green Chem. Lett. Rev. **8** (3–4), 1–12 (2015). doi:10.1080/17518253.2015.1065348
[29] R. Zarifeh, A. Karim, A. Karam and S. Khalloufi, Waste. **1**, 775 (2023). doi:10.3390/waste1030046
[30] M.M. Hamed, M. Holiel and Y.F. El-Aryan, J. Mol. Liq. **242**, 722 (2017). doi:10.1016/j.molliq.2017.07.035
[31] P. Lestari1, G. Purwiandono, S. Pramayshela and E. Siswoyo, J. Ecol. Eng. **25** (1), 229 (2024). DOI: 10.12911/22998993/175199
[32] M.A. El Kassimi, Y. Achour, M. El Himri, R. Laamari and M. El Haddad, Biointerface. Res. Appl. Chem. **11**, 12717–12731 (2021). doi:10.33263/BRIAC115.1271712731
[33] J.M. Salman and K.A. AL-Saad, Int. J. Chem. Sci. **10**, 677 (2012).
[34] M.N. Sepehr, A. Amrane, K.A. Karimaian, M. Zarrabi and H.R. Ghaffari, J.Taiwan Inst. Chem. Eng. **45** (2), 635 (2014). doi:10.1016/j.jtice.2013.07.005
[35] J. Qi, B. Li, P. Zhou, X. Su, D. Yang, J. Wu, W. Zixuan and X. Liang, Sci Rep. **13** (1), 135 (2023). doi:10.1038/s41598-023-27414-9
[36] V.K. Kumar, Chem. Africa. **7** (2), 953 (2024). doi:10.1007/s42250-023-00818-w
[37] K.K. Kebede, T.G. Melak and F. Asere, Sci. World J. 2022 (1), 7554133 (2022). doi:10.1155/2022/7554133
[38] Y.X. Liu, F.M. Zou, J. Khoso, Y.P. Liu, X.Y. Jiang, J.G. Peng and S. Yu, Molecules. **28** (2), 639 (2023). doi:10.3390/molecules28020639
[39] S. Indah, D. Helard, B. Primasari, T. Edwin and R.H. Putra, MATEC Web Conf., 2019 pp. 6009. doi:10.1051/matecconf/201927606009 **276**.
[40] M.T. Angaji, A.Z. Zinali1 and N.T. Qazvini, WJNSE. **3** (04), 161 (2013). doi:10.4236/wjnse.2013.34019
[41] F. Kooli, Y.Z. Khimyak, S.F. Alshahateet and F. Chen, Langmuir. **21** (19), 8717 (2005). doi:10.1021/la050774z
[42] L. Xu, J. Zhang, J. Ding, T. Liu, G. Shi, X. Li, W. Dang, Y. Cheng and R. Guo, Minerals. **10** (1), 72 (2020). doi:10.3390/min10010072
[43] Y. Zhang, D. Shao, J. Yan, X. Jia, Y. Li, P. Yu and T. Zhang, Sichuan Basin, China, JNGGS. **1** (3), 213 (2016). doi:10.1016/j.jnggs.2016.08.002
[44] Y. Yang, J. Zhang, L. Xu, P. Li, Y. Liu and W. Dang, ACS Omega. **7** (11), 9229 (2022). doi:10.1021/acsomega.1c05779
[45] M.N. Sepehr, V. Sivasankar, M. Zarrabi and M.S. Kumar, Chem. Eng. J. **228**, 192 (2013). doi:10.1016/j.cej.2013.04.089
[46] E.A. Abdel-Galil, A.B. Ibrahim and W.M. El-Kenany, Desalin Water. Treat. **226**, 303 (2021). doi:10.5004/dwt.2021.27261
[47] M. Sepehr, M. Zarrabi, H. Kazemian, A. Amrane, K. Yaghmaian and H.R. Ghaffari, Appl. Surf. Sci. **274**, 295 (2013). doi:10.1016/j.apsusc.2013.03.042
[48] A.V. Radha, L. Lander, G. Rousse, J.M. Tarascon and A. Navrotsky, J. Mater. Chem. A. **3** (6), 2601 (2015). doi:10.1039/C4TA05066E
[49] E.A. Abdel-Galil, A.S. Tourky and A.E. Kasem, Appl. Radiat. Isot. **156**, 109009 (2020). doi:10.1016/j.apradiso.2019.109009
[50] L. Zhang, X. Sun, Y. Song, X. Jiang, S. Dong and E. Wang, Langmuir. **22** (6), 2838 (2006). doi:10.1021/la052822l
[51] V. Vats, G. Melton, M. Islam and V.V. Krishnan, J. Hazard. Mater. **448**, 130862 (2023). doi:10.1016/j.jhazmat.2023.130862
[52] E.A. Abdel-Galil, M.A. Eid and R.S. Hassan, Particulate Sci. Technol. **38** (1), 113 (2020). doi:10.1080/02726351.2018.1520764

[53] Y.F. El-Aryan, H. El-Said and E.A. Abdel-Galil, Radiochemistry. **56** (6), 614 (2014). doi:10.1134/S106636221406006X
[54] S.A. Khan, T.A. Khan, S.S. Alharthi, G. Zhu, Y. Zhang and H. Pang, Int. J. Biol. Macromol. **282**, 137049 (2024). doi:10.1016/j.ijbiomac.2024.137049
[55] S.A. Khan, A. Manchanda and T.A. Khan, ChemistrySelect. **9** (15), e202304927 (2024). doi:10.1002/slct.202304927
[56] T. Karthikeyan, S. Rajgopal and L.R. Miranda, J. Hazard. Mater. **124** (1–3), 192 (2005). doi:10.1016/j.jhazmat.2005.05.003
[57] F. Elisabetta, L. Alessandra, S. Carlo and C. Attilio, Chem. Eng J. **156** (2), 264 (2010). doi:10.1016/j.cej.2009.10.015
[58] K. Malwade, D. Lataye, V. Mhaisalkar, S. Kurwadkar and D. Ramirez, Int. J. Environ. Sci. Technol. **13** (9), 2107–2116 (2017). doi:10.1007/s13762-016-1042-z
[59] Y. Peng, F. Mingde, Y. Dan, H. Hongping, L. Dong and Y. Aihua, J Hazard Mater. **166** (2–3), 821 (2009). doi:10.1016/j.jhazmat.2008.11.083
[60] K.G. Pranab, J Hazard Mater. **171** (1–3), 116 (2009). doi:10.1016/j.jhazmat.2009.05.121
[61] E. Mekonnen, M. Yitbarek and T.R. Soreta, S. Afr. J. Chem. **68**, 45 (2015). doi:10.17159/0379-4350/2015/v68a7
[62] A.Z. Zainul, S. Marlini, M. Nurfadilah and A.A. Wan, Desalination. **244** (1–3), 109 (2009). doi:10.1016/j.desal.2008.05.018